Applied Catalysis B: Environmental 123–124 (2012) 174–181

Contents lists available at SciVerse ScienceDirect

Applied Catalysis B: Environmental

journal homepage: www.elsevier.com/locate/apcatb

Comparative study on the mechanism in photocatalytic degradation of different-type organic dyes on SnS_2 and CdS

Xi Li [a], Jian Zhu [a], Hexing Li [a,b,*]

[a] Department of Chemistry, Shanghai Normal University, Shanghai 200234, China
[b] Department of Chemistry, Shanghai University of Electric Power, Shanghai 200090, China

ARTICLE INFO

Article history:
Received 15 January 2012
Received in revised form 4 April 2012
Accepted 8 April 2012
Available online 24 April 2012

Keywords:
SnS_2
CdS
Organic dye
Photoreduction
Photooxidation

ABSTRACT

The photocatalytic performances of the SnS_2 and the CdS under the irradiation of visible light were investigated by using different organic dyes as reactants. The photodegradation of organic dyes containing N=N double bond on the SnS_2 followed a reduction mechanism with photoelectrons *via* the Sn^{IV}/Sn^{II} transition while the photodegradation of organic dyes containing N=N double bond on the CdS and the photodegradation of organic dyes without N=N double bond on either the SnS_2 or the CdS followed an oxidation mechanism with $^{\bullet}O_2^-$ and $^{\bullet}OH$ radicals. The SnS_2 exhibited much higher activity than the CdS during the photocatalytic degradation of organic dyes containing N=N double bond, since the reduction of reactant molecules on the SnS_2 surface was much faster than the migration of either the $^{\bullet}O_2^-$ or the $^{\bullet}OH$ radicals. However, the SnS_2 displayed even lower activity than the CdS in the photocatalytic degradation of other organic dyes without N=N double bond, since all these reactions followed the oxidation mechanism and the SnS_2 displayed a lower efficiency than the CdS in producing $^{\bullet}O_2^-$ or $^{\bullet}OH$ radicals due to the presence of the Sn^{IV}/Sn^{II} transition.

1. Introduction

Photocatalysis has been widely studied owing to its potential applications in cleaning environment and producing H_2 energy *via* splitting water [1,2]. Organic dyes, typically as azo dyes and fluorescein dyes, have been reported to be highly cytotoxic for the mammalian tissues [3,4]. Such dye molecules are normally difficult to be decomposed by natural means [5]. Various methods, such as adsorption, advanced oxidation processes (AOPs), biological treatment, electrocatalysis and photocatalysis [6–10], have been developed to remove organic dyes, in which the photocatalytic degradation of organic pollutants has received increasing interest owing to the absence of secondary pollution and the low cost by using solar light [11]. TiO_2 photocatalyst has been most frequently employed for the oxidative degradation of organic compounds due to its cheapness, non-toxicity, and stability *etc.* [12]. However, TiO_2 could be activated only by ultraviolet light ($\lambda < 387$ nm) due to its wide band gap ($E_g \approx 3.2$ eV), which greatly limits its practical application since only less than 5% ultraviolet lights are present in total sunlight. Metal sulfides, such as CdS, In_2S_3, SnS_2, Sb_2S_3, $Zn_xCd_{1-x}S$, $ZnIn_2S_4$, $SnIn_4S_8$ and $In(OH)_xS_y$ [13–20], have been proved as visible photocatalysts owing to their narrow energy band gaps, and have been widely used in photocatalytic degradation of organic dyes, especially methyl orange (MO) and rhodamine B (RhB). Up to now, most studies are focused on the CdS. The SnS_2 exhibits relatively higher stability than the CdS against oxidation and photocorrosion, however, its photocatalytic performances are seldom studied [21,22], possibly due to the poor activity under most cases. Moreover, the excellent photocatalytic activity has not yet been found in degradation of certain organic compounds.

In the present work, we reported for the first time that the SnS_2 exhibited much higher activity than the CdS during visible light induced photocatalytic degradation of organic dyes containing N=N double bond. In contrast, the SnS_2 displayed even lower activity than the CdS in the photocatalytic degradation of other organic dyes without N=N double bond. Based on the detailed characterizations, two kinds of reaction mechanisms were recognized. The degradation of organic dyes containing N=N double bond followed a reduction mechanism with photoelectrons *via* the Sn^{IV}/Sn^{II} transition on the SnS_2 and an oxidation mechanism with $^{\bullet}O_2^-$ and $^{\bullet}OH$ radicals, which could account for the higher activity of the SnS_2 than that of the CdS since the reduction of reactant molecules on the SnS_2 surface was more rapid than the migration of the $^{\bullet}O_2^-$ and the $^{\bullet}OH$ radicals. The degradation of organic dyes without N=N double bond on either the SnS_2 or the CdS followed the same mechanism of oxidation and the SnS_2 exhibited lower activity than the CdS due to the effect of the Sn^{IV}/Sn^{II} transition, which decreased the formation of $^{\bullet}O_2^-$ and $^{\bullet}OH$ radicals.

* Corresponding author at: Department of Chemistry, Shanghai Normal University, Shanghai 200234, China. Tel.: +86 21 64322272; fax: +86 21 64322272.
E-mail address: Hexing-Li@shnu.edu.cn (H. Li).

0926-3373/$ – see front matter © 2012 Elsevier B.V. All rights reserved.
http://dx.doi.org/10.1016/j.apcatb.2012.04.009

2. Experimental

2.1. Photocatalyst preparation

SnS_2 photocatalyst was prepared by a hydrothermal method [23]. In a typical run of synthesis, 2.5 mmol $SnCl_4{\cdot}5H_2O$ and 10 mmol thioacetamide (TAA) were dissolved in 40 mL deionized water. The solution was transferred to a 50 mL Teflon-lined stainless steel autoclave and maintained at 200 °C for 24 h. The product was collected by centrifugation, followed by washing thoroughly with deionized water and absolute ethanol in order. The final product was dried at 80 °C in vacuum for 3 h. The CdS was commercially available from Aladdin Chemical Reagent Corporation and used without further treatment.

2.2. Characterizations

The surface electronic states were analyzed by X-ray photoelectron spectroscopy (XPS, PerkinElmer PHI 5000). All the binding energy values were calibrated by using C_{1s} = 284.6 eV as a reference. The sample structure was determined by X-ray diffraction (XRD, Rigacu D/Max-2000, monochromatic CuKα radiation), field emission scanning electron microscopy (FESEM, HITACHI S4800), high-resonance transmission electron microscopy (HRTEM) and selective area electronic diffraction (SAED) collected on a JEOL JEM2100, and N_2 adsorption–desorption (Quantachrome NOVA 4000e, at 77 K). The optical properties were determined by UV–visible diffuse reflectance spectrum (Cary 500, Varian) and photoluminescence spectrum (PLS, Varian Cary-Eclipse 500). Liquid chromatography–mass spectrometry (HPLC–MS, Angilent 1200) was used to monitor the photocatalytic process. Electron spin resonance (ESR) spectrum was obtained on a Bruker model ESP 300E electron paramagnetic resonance spectrometer.

2.3. Photocatalytic activity tests

The visible light driven photocatalytic degradation reactions of two kinds of organic dyes with and without N=N double bond were used as probes to evaluate catalytic performances of the SnS_2 and the CdS. All reactions were carried out at 30 °C in a 100 mL quartz reactor. During the photocatalytic degradation of MO, 20 mg photocatalyst was added into 50 mL aqueous solution containing 6.0×10^{-5} mol/L MO. The mixture was allowed to stir for enough time to reach the adsorption–desorption equilibrium. Then, the reactions were initiated by irradiating with a 300 W Xenon lamp (CHF-XM300) located 15 cm away from the solution. A cutoff filter was equipped to remove UV light with wavelength (λ) below 420 nm. After reaction, the concentration of unreacted MO in solution was determined by UV–visible spectrophotometer (UV 7504/PC) at its characteristic wavelength and from which, the degradation yield could be calculated. The photocatalytic degradation of rhodamine B (RhB) was conducted in the same reaction conditions except for the use of 50 mg photocatalyst. The reproducibility of the results was checked by repeating each reaction at least three times and was found to be within acceptable limits (±5%).

3. Results and discussion

3.1. Structural characteristics

The XPS spectra (Fig. S1) demonstrated that all the Sn and Cd species were present in +4 and +2 oxidation states, while both of S species were present in −2 state, corresponding to binding energies of 486.7, 405.2 and 161.2 eV in $Sn_{3d5/2}$, $Cd_{3d5/2}$ and S_{2p} levels, respectively [15,24]. The XRD peaks (Fig. 1) revealed that both the SnS_2 and the CdS were present in hexagonal crystal structure (JCPDS card Nos. 23-0677 and 65-3414), corresponding to relatively uniform nanosheets observed from the FESEM images (Fig. S2). Meanwhile, the HRTEM and the attached SAED images (Fig. S3) displayed well-resolved diffraction cycles and crystal lattices (0.182 nm and 0.382 nm for (1 1 0) and (1 0 0) facets in the SnS_2 and 0.318 nm for the (1 0 1) facets in the CdS) characteristic of highly crystallized hexagonal crystals [22,25], which was in good accordance with the XRD patterns. Based on the width of principal XRD peak, the average crystal sizes of the SnS_2 and the CdS were respectively calculated as 46 and 21 nm from the Scherrer equation (see Table 1). The UV–vis DRS spectra in Fig. 2 revealed that both the SnS_2 and the CdS displayed response in the visible region. According to the UV–vis DRS spectra, the band gap of SnS_2 was estimated to be 2.0 eV, whereas that of CdS was 2.3 eV, calculated by the method [26]. The SnS_2 displayed a narrow band gap than the CdS (see Table 1).

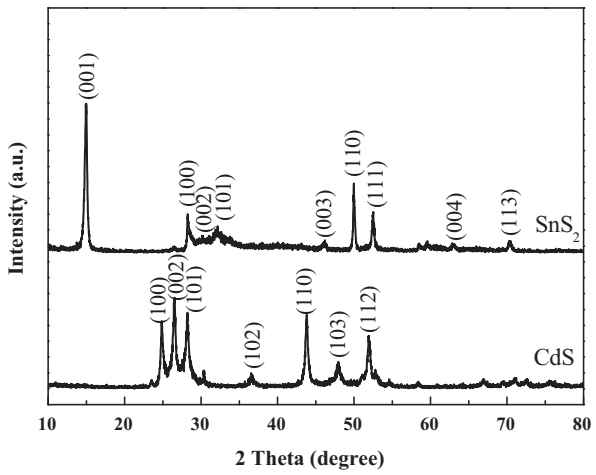

Fig. 1. XRD patterns of SnS_2 and CdS.

Table 1
Structural and optical parameters of SnS_2 and CdS.

Sample	Crystal size (nm)	Band gap (eV)	S_{BET} (m^2/g)	D_P (nm)	V_P (cm^3/g)
SnS_2	46	2.0	56	19	0.27
CdS	21	2.3	31	9.2	0.070

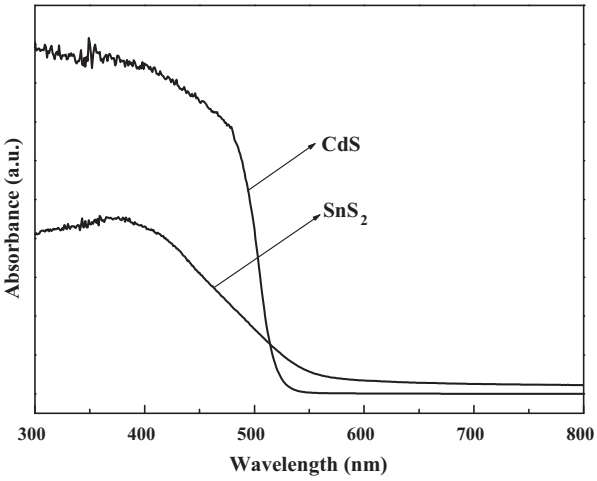

Fig. 2. UV–vis DRS spectra of SnS_2 and CdS.

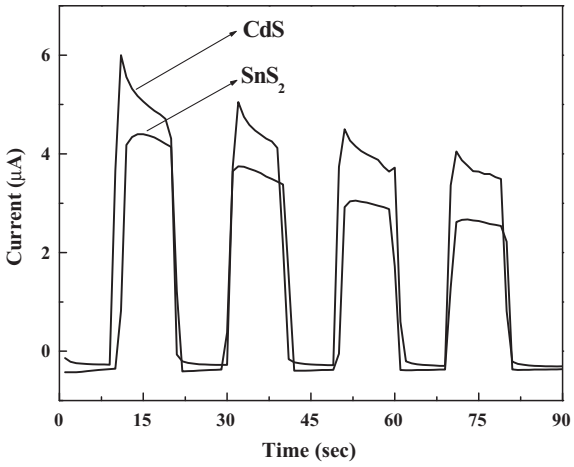

Fig. 3. The response of photo-induced pulse current on SnS_2 and CdS.

Fig. 3 showed the response of photo-induced pulse current on the SnS_2 and the CdS. In spite of the narrower band gap, the SnS_2 still exhibited lower strength of the photo-induced current than the CdS, which could mainly attribute to the higher recombination probability between photoelectron and holes. The PLS spectra (Fig. S4) clearly demonstrated that the SnS_2 displayed stronger peaks around 500 nm than the CdS, indicating the higher recombination between photoelectrons and holes [27], which could also successfully account for the much stronger absorbance of the CdS in ultraviolet area than that of the SnS_2.

Other structural parameters including the specific surface areas (S_{BET}), the pore diameter (D_P), and the pore volume (V_P) were calculated from the N_2 adsorption–desorption isotherms (Fig. S5). As shown in Table 1, although the SnS_2 had the bigger crystal size, it still exhibited much higher S_{BET} than the CdS, which could be mainly attributed to the presence of porous structure, corresponding to the large D_P and V_P.

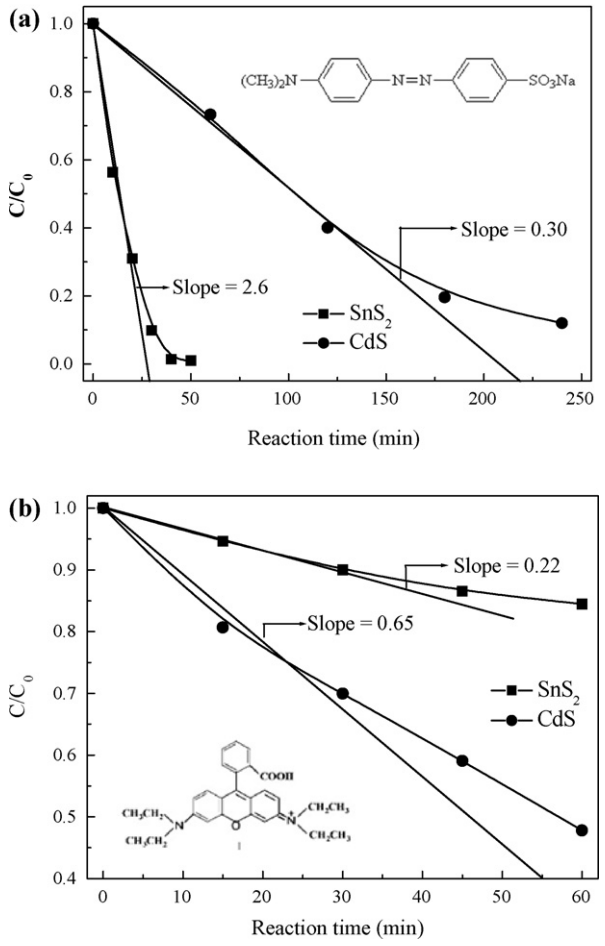

Fig. 4. Reaction profiles of (a) MO and (b) RhB photocatalytic degradation. Reaction conditions: 20 mg (a) or 50 mg (b) photocatalyst, 50 mL 6.0×10^{-5} mol/L organic dyes, a 300 W Xenon lamp ($\lambda > 420$ nm), reaction temperature = 30 °C.

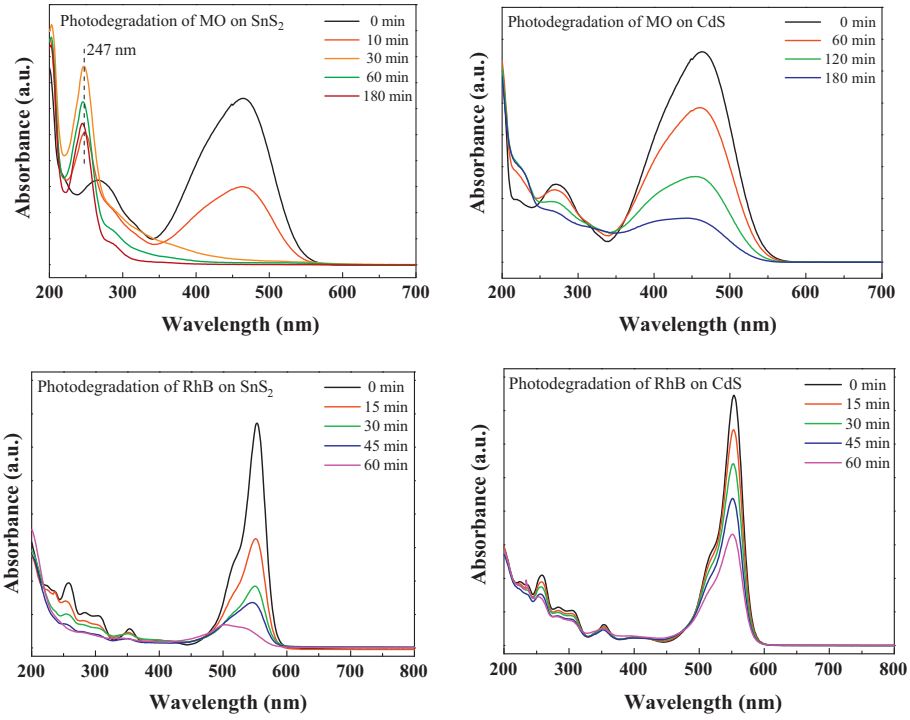

Fig. 5. Time dependence of the UV–vis spectra in photodegradation of MO and RhB on SnS_2 and CdS photocatalysts. Reaction conditions are given in Fig. 4.

3.2. Photocatalytic performance

The photocatalytic performances of the SnS_2 and the CdS were examined and compared by using photodegradation of MO and RhB as probes. As shown in Fig. 4a, the SnS_2 exhibited much higher activity than the CdS during photocatalytic degradation of MO under visible light irradiation. Calculation from the tangent slope demonstrated that the initial rate of the SnS_2 was nearly 9 times as the CdS. However, to our surprise, the SnS_2 displayed even slightly lower activity than the CdS during photocatalytic degradation of RhB under visible light irradiation. As shown in Fig. 4b, the initial rate of the CdS was almost 3 times as the SnS_2.

To elucidate the different performances of the SnS_2 photocatalyst in degrading MO and RhB, the reaction mechanism was thus examined. Firstly, the UV–vis spectra (Fig. 5) revealed that, besides MO molecule with the characteristic absorbance wavelength (λ) around 464 nm which gradually decreased with the increased reaction time, a byproduct appeared at characteristic λ of 247 nm was observed during the photodegradation of MO on either the SnS_2 or CdS photocatalyst. With the reaction proceeding, the concentration of the byproduct first increased rapidly and then decreased slowly on the SnS_2 photocatalyst. However, the concentration of the byproduct was very low on the CdS and decreased monotonously during the reaction. These results demonstrated that the photocatalytic degradation of MO on the SnS_2 and the CdS photocatalysts followed different mechanisms, while the photodegradation of RhB on either the SnS_2 or the CdS followed the similar reaction mechanism, corresponding to the identical change of the UV–vis spectra with the increase of reaction time. The reaction mechanism could be further investigated by HPLC–MS to determine the reaction intermediates. As shown in Fig. 6, the degradation of MO on the SnS_2 displayed different byproducts (m/z values) from the CdS photocatalysts, corresponding to the different reaction mechanisms. The degradation of RhB on both the SnS_2 and the CdS photocatalysts exhibited the same byproducts, suggesting that the reaction followed the same mechanism.

Based on the formation of various byproducts (m/z values) and the change of their contents during the reaction process (Fig. S6), we could conclude the possible pathway of MO and RhB photodegradation on SnS_2 and CdS respectively. The photodegradation of MO on the SnS_2 and the CdS photocatalysts followed different mechanisms. Particularly the most byproduct with $m/z = 172$ on SnS_2 was confirmed by the MS spectrum of the standard 4-aminobenzene

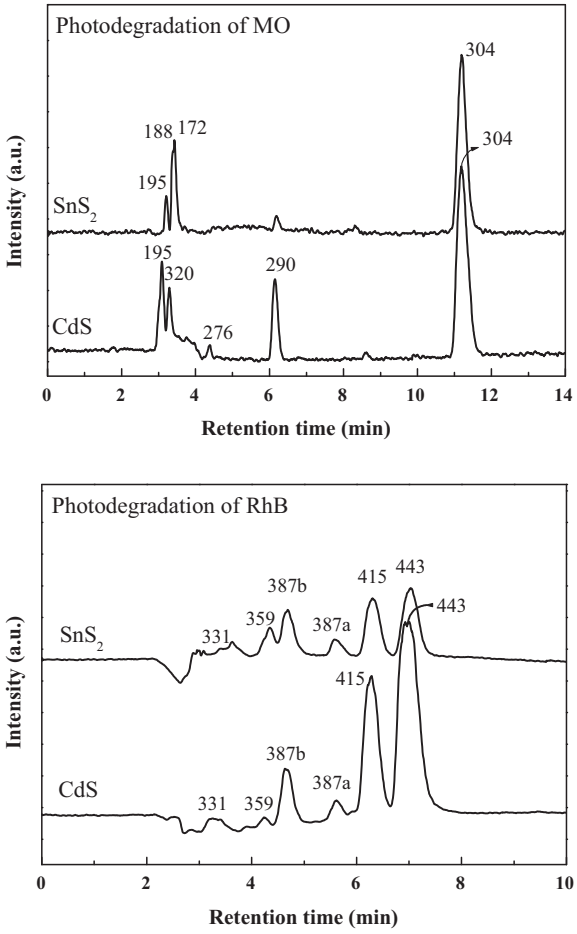

Fig. 6. HPLC–MS spectra of MO and RhB photocatalytic degradation on SnS_2 and CdS photocatalysts. The numbers on the peaks represent the m/z values. Reaction conditions are given in Fig. 4.

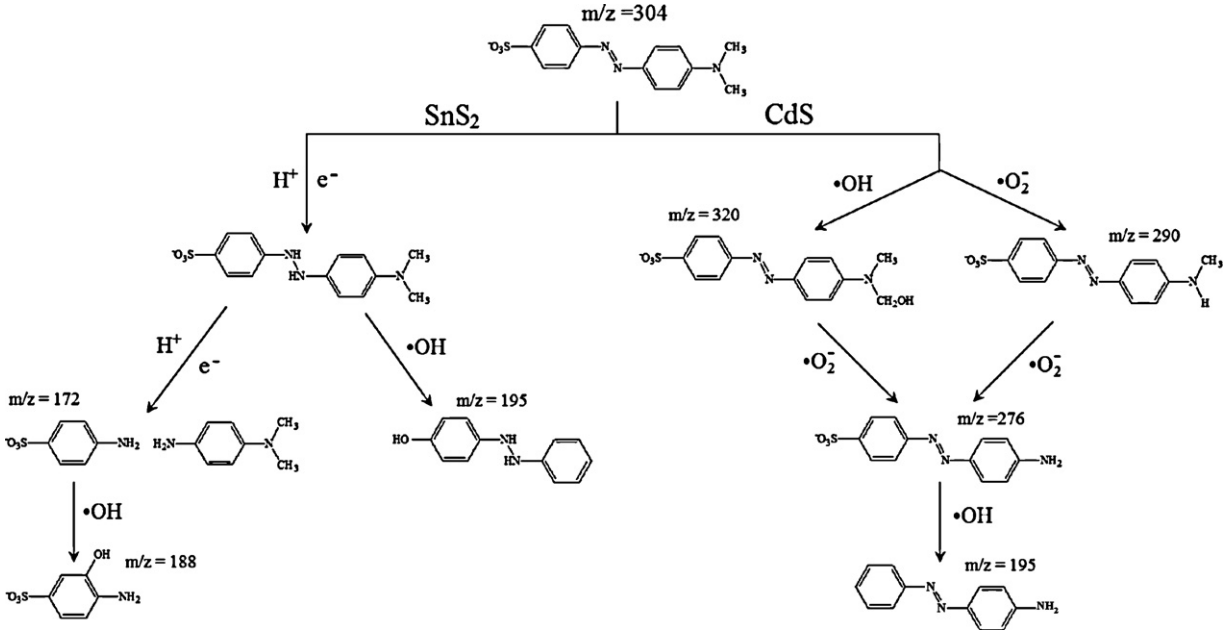

Scheme 1. The plausible reaction mechanisms of the MO degradation on SnS_2 and CdS photocatalysts.

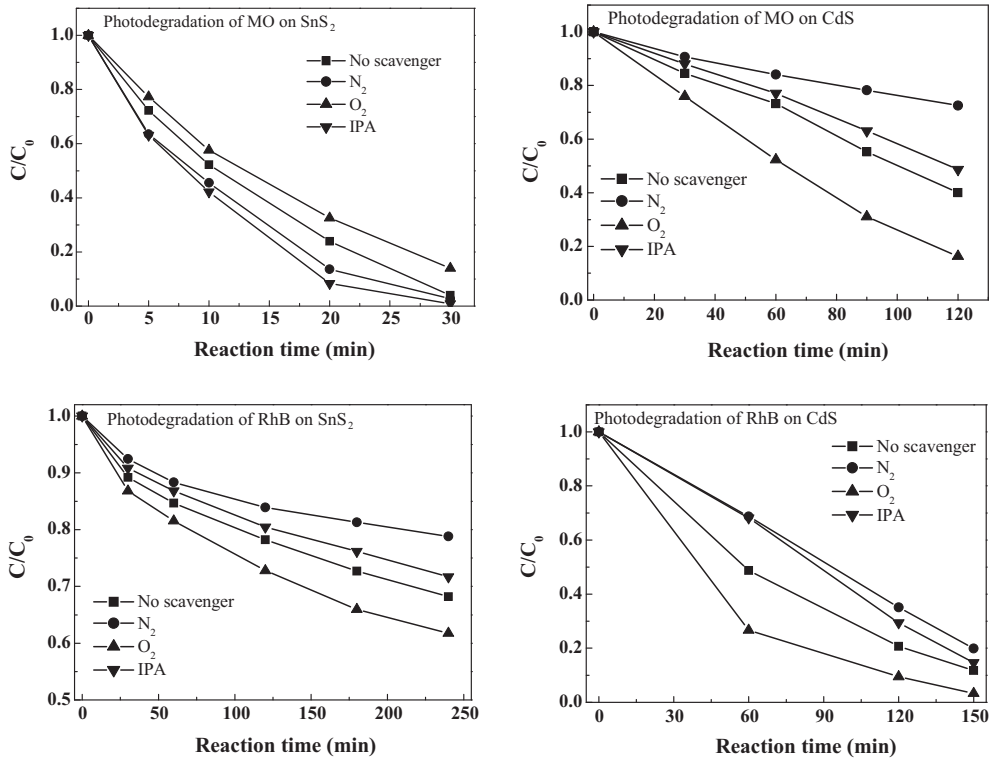

Fig. 7. Effects of various scavengers on the photocatalytic efficiencies of SnS_2 and CdS photocatalysts in the MO and RhB degradation. Reaction conditions are given in Fig. 4.

sulfonic acid solution (Fig. S7), and also was corresponded to the byproduct at around $\lambda = 247$ nm in UV–vis spectrum (Fig. S7). The MO degradation on the SnS_2 photocatalyst followed a reduction mechanism in which the photoelectrons directly reduced the N=N double bond [28,29], followed by the subsequent oxidation by other active sites including $^{\bullet}O_2^-$ and/or $^{\bullet}OH$ radicals, as possibly illustrated in Scheme 1. However, the MO photodegradation on the CdS followed an oxidation mechanism, that was, the photoelectrons first reacted with O_2 and proton to produce $^{\bullet}O_2^-$ and/or $^{\bullet}OH$ radicals [30], followed by oxidizing the MO molecule into various byproducts. Unlike the MO photodegradation, the RhB photodegradation on either the SnS_2 or the CdS followed the same oxidation mechanism, possibly as illustrated in Scheme 2.

The reduction and oxidation mechanisms during photocatalytic degradation of MO and RhB could be further confirmed by the following controlled experiments in which the dissolved O_2 and isopropyl alcohol (IPA) acted as scavengers for capturing photoelectrons and $^{\bullet}OH$ radicals, respectively [31,32]. As shown in Fig. 7, during the photocatalytic degradation of MO on the SnS_2, the reaction was abruptly inhibited by O_2. Correspondingly, the MO degradation rate could be significantly enhanced by purging N_2 flow into the solution to exclude dissolved O_2. Meanwhile, the reaction rate could also be accelerated by adding IPA to capture $^{\bullet}OH$ radicals. In contrast, during the photocatalytic degradation of MO on the CdS, the reaction rate increased by purging O_2 flow and decreased by either purging N_2 flow into the solution to exclude dissolved O_2 or adding IPA to capture $^{\bullet}OH$ radicals. The effects of various scavengers on the reaction rate of RhB photocatalytic degradation on either the SnS_2 or the CdS photocatalysts were almost the same, *i.e.*, the O_2 flow promoted while the N_2 flow and the IPA inhibited the RhB photodegradation. These results demonstrated that the MO photocatalytic degradation on the SnS_2 proceeded through a reduction of the N=N double bond by photoelectrons while the MO photocatalytic degradation on the CdS and the RhB photodegradation on either the SnS_2 or the CdS followed the oxidation mechanism with the $^{\bullet}O_2^-$ and $^{\bullet}OH$ radicals as active species, as confirmed by the ESR spectra of DMPO-$^{\bullet}O_2^-$ and DMPO-$^{\bullet}OH$ (see Fig. 8). Thus, the photocatalytic degradation of MO on the SnS_2 could be abruptly inhibited by purging O_2 flow since the dissolved O_2 could effectively capture

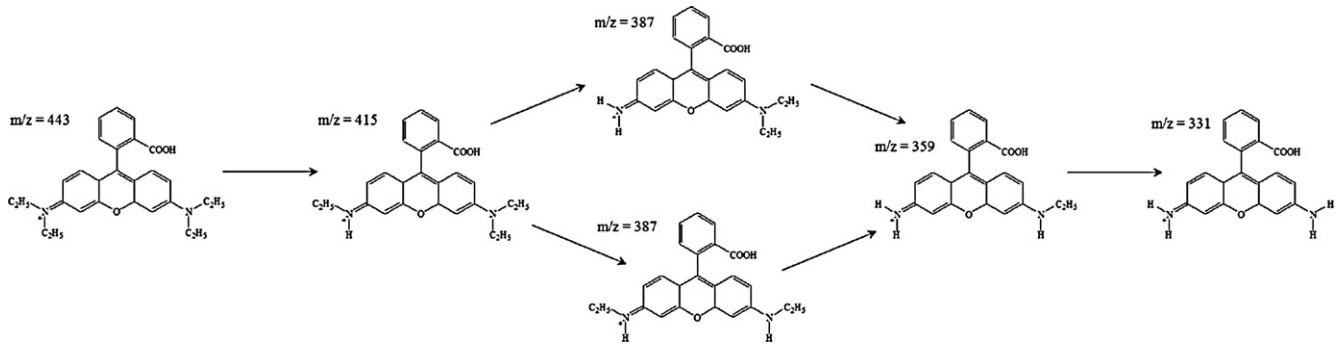

Scheme 2. A plausible mechanism of the RhB degradation on SnS_2 and CdS photocatalysts.

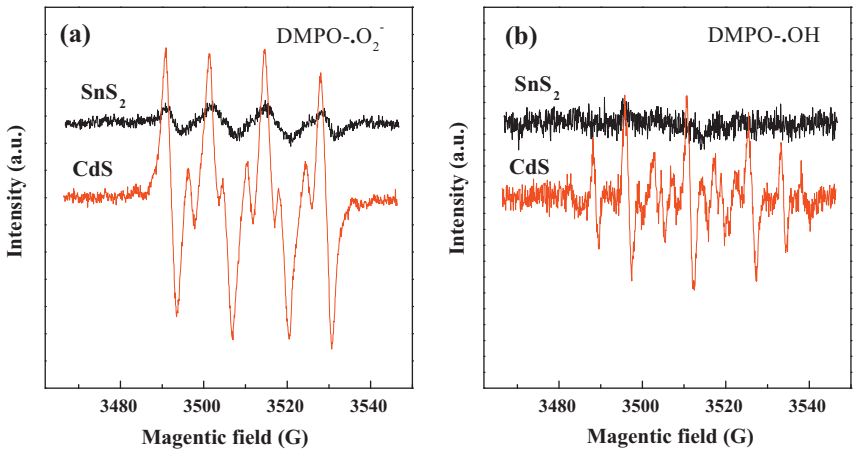

Fig. 8. ESR spectra of (a) DMPO-•O_2^- and (b) DMPO-•OH obtained from SnS_2 and CdS photocatalysts under visible light irradiation ($\lambda > 420$ nm).

Table 2
The photodegradation of various organic dyes on SnS_2 and CdS.

Entry	Organic dye	Molecular structure	Degradation yield (%)	
			SnS_2	CdS
1[a]	Methyl orange (MO)	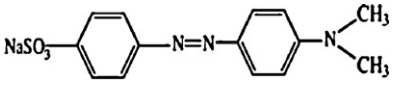	99	16
2[a]	Congo red (CR)	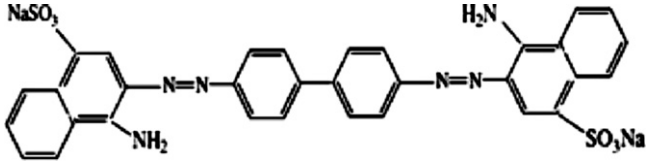	90	84
3[a]	Orange II (OII)	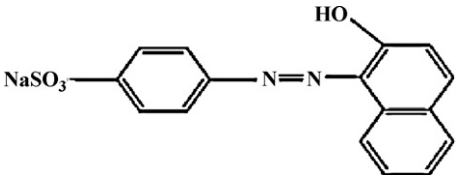	44	26
4[b]	Rhodamine B (RhB)	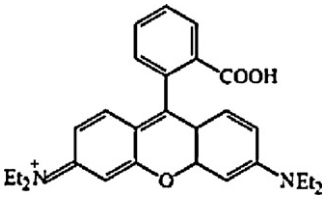	10	31
5[b]	Malachite green (MG)	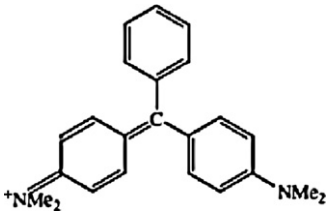	15	95
6[c]	Methylene blue (MB)	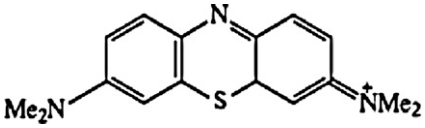	30	51

[a] 20 mg catalyst, 50 mL aqueous solution containing 6.0×10^{-5} mol/L organic dye, $\lambda > 420$ nm, reaction time (t) = 30 min, temperature (T) = 30 °C.
[b] 50 mg catalyst, 50 mL aqueous solution containing 6.0×10^{-5} mol/L organic dye, $\lambda > 420$ nm, t = 30 min, T = 30 °C.
[c] 20 mg catalyst, 50 mL aqueous solution containing 6.0×10^{-5} mol/L organic dye, $\lambda > 420$ nm, t = 30 min, T = 30 °C.

photoelectrons. This could also account for the promoting effects of either the N_2 flow or the IPA since they could effectively exclude dissolved O_2 and capture •OH radicals, which could thus effectively prevent them from combination with the photoelectrons ($e^- + O_2 \rightarrow {}^\bullet O_2^-$; ${}^\bullet O_2^- + 2H^+ + e^- \rightarrow H_2O_2$; $H_2O_2 + e^- \rightarrow {}^\bullet OH + OH^-$) [30]. On the contrary, since the photodegradation of MO on the CdS and the photodegradation of RhB on either the SnS_2 or the CdS followed the oxidation mechanism, the presence of O_2 flow could greatly enhance the activity owing to the formation of more ${}^\bullet O_2^-$ and •OH radicals which acted as powerful oxidizing agents for the oxidative degradation of MO or RhB molecules. Accordingly, the presence of either the N_2 flow or the IPA was harmful for the reaction since they could retard the formation of ${}^\bullet O_2^-$ radicals by excluding dissolved O_2 and also capture •OH radicals. In addition, we could see that the inhibiting effect of the N_2 flow was much stronger than the IPA, suggesting that the ${}^\bullet O_2^-$ radicals played a more important role than the •OH radicals in oxidizing degradation of either MO or RhB, which was consistent with the relatively stronger DMPO-${}^\bullet O_2^-$ peaks than the DMPO-•OH peaks in the ESR spectra observed from either the SnS_2 or the CdS (see Fig. 8).

The different mechanisms of MO photodegradation on the SnS_2 and the CdS could be understood by considering their potentials of the conduction band (E_{CB}) and the valence band (E_{VB}), which could be calculated by the following empirical equation [33,34]:

$$E_{CB} = X - E_e - 0.5E_g$$

$$E_{VB} = X - E_e + 0.5E_g$$

where X refers to the electronegativity of the semiconductor and determined as 4.66 eV [35] and 5.04 eV [34] for the SnS_2 and the CdS, respectively. While, E_e refers the energy of free electron with respect to the hydrogen scale and determined as 4.5 eV [34]. Based the E_g values determined by aforementioned UV–vis DRS spectra (see Table 1), the E_{CB} and E_{VB} of the semiconductors were determined as −0.83 and 1.2 V on the SnS_2 and as −0.61 and 1.69 V on the CdS, respectively. The redox potential in solid of the semiconductors could be roughly estimated according to those determined in aqueous solution ($E^\circ_{Sn(IV)/Sn(II)} = 0.15$ V [36] and $E^\circ_{Cd(II)/Cd(0)} = -0.41$ V [37]). Since the redox potential of $O_2/{}^\bullet O_2^-$ ($E^\circ = -0.33$ V) [38] was more negative than that of Sn^{IV}/Sn^{II} but more positive than that of Cd^{II}/Cd^0, Sn^{IV} could be preferentially reduced to Sn^{II} by the photoelectrons while O_2 was preferentially reduced to ${}^\bullet O_2^-$ on CdS, and their individual potential positions were illustrated in Scheme 3. Then, Sn^{II} could reduce N=N double bond and returned to Sn^{IV} while ${}^\bullet O_2^-$ could oxidize the MO molecule. Accordingly, less ${}^\bullet O_2^-$ and •OH were generated on SnS_2 than CdS, as shown in Fig. 8. The Sn^{IV}/Sn^{II} transition was considered to play a role of photoelectrons transfer to reduce the reactant molecules, which was similar to the Bi^{III}/Bi^{V} transition as reported [39]. As a result, the photoreduction reaction was predominant on SnS_2 in the photocatalytic degradation of MO while

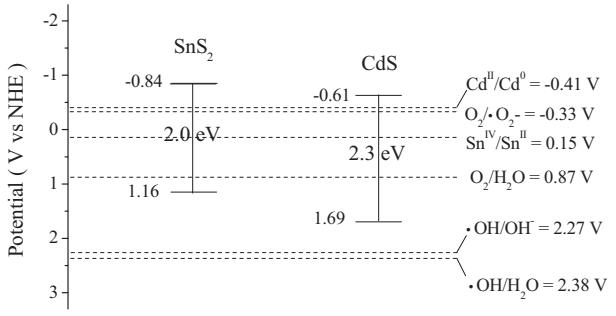

Scheme 3. Energy levels of SnS_2 and CdS semiconductors.

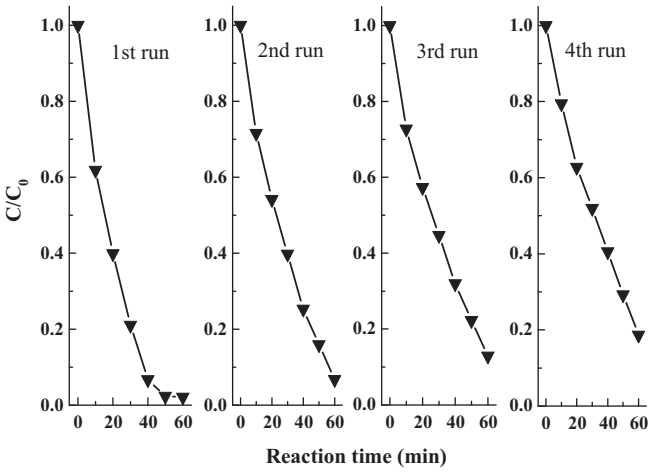

Fig. 9. Recycling test of SnS_2 in photocatalytic degradation of MO. Reaction conditions are given in Fig. 4.

the photooxidation occurred on CdS. This could account that SnS_2 exhibited much higher rate in photocatalytic degradation of MO than the CdS since the reduction of reactant molecules on the SnS_2 surface was much faster than the migration of either the ${}^\bullet O_2^-$ or the •OH radicals. In contrast, the SnS_2 displayed lower rate in photocatalytic degradation of RhB than the CdS since the reactions on both these two photocatalysts followed the same oxidation mechanism and the CdS could produce the ${}^\bullet O_2^-$ and the •OH radicals more efficiently than the SnS_2. The above results could also be observed during the photocatalytic degradation of other organic dyes. As shown in Table 2, the SnS_2 exhibited higher activity than the CdS during the photocatalytic degradation of those organic dyes containing N=N double bond, but showed lower activity during the photocatalytic degradation of other organic dyes without N=N double bond, suggesting that the photocatalysis *via* the Sn^{IV}/Sn^{II} transition with photoelectrons proceeded much more rapid than that *via* oxidation. According to the potential diagram in Scheme 3, the photo-induced holes on either SnS_2 or CdS photocatalyst exhibited lower potential than both the $^\bullet OH/H_2O$ and the $^\bullet OH/OH^-$, implying that they could not oxidize either H_2O or OH^- directly. Most studies revealed that the holes could directly oxidize sulfide ions in CdS, leading to the rapid deactivation due to photocorrosion of CdS [40,41]. However, besides the higher photoactivity, the SnS_2 also displayed stronger stability against photocorrosion than the CdS in the photodegradation of MO. As shown in Fig. 9, the SnS_2 could be used repetitively for 3 times in the photocatalytic degradation of MO with only little decrease in the activity, but the CdS displayed an abrupt deactivation even during the second cycle of photocatalytic reactions. According to the ICP analysis, only less than 0.23% SnS_2 species was leached off. Meanwhile, the XPS analysis (Fig. S8) revealed that no significant peak shifts were observed in the used SnS_2 photocatalyst. However, the CdS showed about 27% leading after the first cycle, obviously due to the photo-induced oxidation. These results demonstrated that only small fraction of photo-induced holes were consumed by oxidizing sulfide ions in SnS_2. Possibly, the left holes were consumed by reacting with either H_2O to O_2 or some intermediate resulted from the degradation of organic compounds.

4. Conclusions

In summary, this work supplied new insights into the photocatalytic mechanism on metal sulfide photocatalysts by using MO-like organic dyes containing N=N double bond as reactants: the reduction route by the transferred photoelectrons *via* the Sn^{IV}/Sn^{II} transition on the SnS_2 and the oxidation route by ${}^\bullet O_2^-$ and/or •OH

radicals on the CdS. The photocatalytic degradation of RhB-like organic dyes without N=N double bond always followed an oxidation route regardless of the photocatalyst employed. The SnS_2 exhibited much higher activity than the CdS in the photodegradation of MO-like organic dyes, since the reduction of reactant molecules on the SnS_2 surface was much faster than the migration of either the $^{\bullet}O_2^-$ or the $^{\bullet}OH$ radicals. However, the SnS_2 showed even lower activity than the CdS in the degradation of RhB-like organic dyes since CdS could produce active species ($^{\bullet}O_2^-$ and/or $^{\bullet}OH$ radicals) more efficiently than the SnS_2 owing to the more oxidative species yielded. Besides the high activity, the photocatalysis *via* photoelectron reduction could also effectively protect the metal sulfide from oxidation, leading to the enhanced durability. We hope that there would be a promising practice for SnS_2 in the treatment of organic dyes under solar light.

Acknowledgment

This work is supported by National Natural Science Foundation of China (20825724), Shanghai Government (10dj1400100, 08GG13), Education Ministry Key Lab of Resource Chemistry, Shanghai Key Lab of Rare Earth Functional Materials. We also thank Dr. Liyan Xie and Shijing Liang from Research Institute of Photocatalysis, Fuzhou University for the ESR measurements.

Appendix A. Supplementary data

Supplementary data associated with this article can be found, in the online version, at http://dx.doi.org/10.1016/j.apcatb.2012.04.009.

References

[1] M. Hoffmann, S.T. Martin, W. Choi, D.W. Bahnemann, Chemical Reviews 95 (1995) 69.
[2] X.B. Chen, S.H. Shen, L.J. Guo, S.S. Mao, Chemical Reviews 110 (2010) 6503.
[3] C.R. Nony, M.C. Bowman, T. Cairns, Journal of Analytical Toxicology 4 (1980) 132.
[4] R.B. Haveland-Smith, R.D. Combes, B.A. Briges, Mutation Research 88 (1981) 1.
[5] M.A. Brown, S.C. De-Vito, Critical Reviews in Environmental Science and Technology 23 (1993) 249.
[6] J. Zhu, S.L. Wang, S.H. Xie, H.X. Li, Chemical Communications 47 (2011) 4403.
[7] H.J. Hsing, P.C. Chiang, E.E. Chang, M.Y. Chen, Journal of Hazardous Materials 141 (2007) 8.
[8] O. Anjaneya, S.Y. Souche, M. Santoshkumar, T.B. Karegoudar, Journal of Hazardous Materials 190 (2011) 351.
[9] G.Q. Zhang, F.L. Yang, M.M. Gao, L.F. Liu, Journal of Physical Chemistry C 112 (2008) 8957.
[10] Z.F. Bian, Y.N. Huo, Y. Zhang, J. Zhu, Y.F. Lu, H.X. Li, Applied Catalysis B 91 (2009) 247.
[11] H. Einaga, S. Futamura, T. Ibusuki, Environmental Science and Technology 35 (2001) 1880.
[12] H.X. Li, Z.F. Bian, J. Zhu, D.Q. Zhang, G.S. Li, Y.N. Huo, H. Li, Y.F. Lu, Journal of the American Chemical Society 129 (2007) 8406.
[13] S.L. Xiong, B.J. Xi, Y.T. Qian, Journal of Physical Chemistry C 114 (2010) 14029.
[14] G.D. Liu, X.L. Jiao, Z.H. Qin, D.R. Chen, CrystEngComm 13 (2011) 182.
[15] Y.Q. Lei, S.Y. Song, W.Q. Fan, Y. Xing, H.J. Zhang, Journal of Physical Chemistry C 113 (2009) 1280.
[16] M. Sun, D.Z. Li, W.J. Li, Y.B. Chen, Z.X. Chen, Y.H. He, X.Z. Fu, Journal of Physical Chemistry C 112 (2008) 18076.
[17] W.J. Li, D.Z. Li, Z.X. Chen, H.J. Huang, M. Sun, Y.H. He, X.Z. Fu, Journal of Physical Chemistry C 112 (2008) 14943.
[18] Z.X. Chen, D.Z. Li, W.J. Zhang, Yu Shao, T.W. Chen, M. Sun, X.Z. Fu, Journal of Physical Chemistry C 113 (2009) 4433.
[19] T.J. Yan, L.P. Li, G.S. Li, Y.J. Wang, W.B. Hu, X.F. Guan, Journal of Hazardous Materials 186 (2011) 272.
[20] S.X. Ge, L.Z. Zhang, Environmental Science and Technology 45 (2011) 3027.
[21] Y.C. Zhang, Z.N. Du, S.Y. Li, M. Zhang, Applied Catalysis B 95 (2010) 153.
[22] W.M. Du, D.H. Deng, Z.T. Han, W. Xiao, C. Bian, X.F. Qian, CrystEngComm 13 (2011) 2071.
[23] C.X. Zhai, N. Du, H. Zhang, D.R. Yang, Chemical Communications 47 (2011) 1270.
[24] P. Thakura, S.S. Joshi, K.R. Patil, Applied Surface Science 257 (2010) 1390.
[25] G.S. Li, D.Q. Zhang, J.C. Yu, Environmental Science and Technology 43 (2009) 7079.
[26] M.A. Butler, Journal of Applied Physics 48 (1977) 1914.
[27] L.Q. Jing, Y.C. Qu, B.Q. Wang, S.D. Li, B.J. Jiang, L.B. Yang, W. Fu, H.G. Fu, J.Z. Sun, Solar Energy Materials and Solar Cells 90 (2006) 1773.
[28] G. Brown, J.R. Darwent, Journal of the Chemical Society, Faraday Transactions I 80 (1984) 1631.
[29] M. Yoon, M. Seo, C. Jeong, J.H. Jang, K.S. Jeon, Chemistry of Materials 17 (2005) 6069.
[30] W.J. Li, D.Z. Li, J.J. Xian, W. Chen, Y. Hu, Y. Shao, X.Z. Fu, Journal of Physical Chemistry C 114 (2010) 21482.
[31] W.J. Li, D.Z. Li, S.G. Meng, W. Chen, X.Z. Fu, Y. Shao, Environmental Science and Technology 45 (2011) 2987.
[32] L.S. Zhang, K.H. Wong, H.Y. Yip, C. Hu, J.C. Yu, C.Y. Chan, P.K. Wong, Environmental Science and Technology 44 (2010) 1392.
[33] M.A. Butler, D.S. Ginley, Journal of the Electrochemical Society 125 (1978) 228.
[34] D.S. Ginley, M.A. Butler, Journal of the Electrochemical Society 125 (1978) 1968.
[35] C.Y. Yang, W.D. Wang, Z.C. Shan, F.Q. Huang, Journal of Solid State Chemistry 182 (2009) 807.
[36] Y.C. Wong, C.T. Wong, New Way Chemistry for Hong Kong A-level, 3rd edition, Manhattan Press (H.K.), Kong Kong, 1998, p. 109.
[37] A.W. Andrews, D.A. Armitage, R.W.C. Broadbank, K.W. Morcom, B.L. Muju, Transactions of the Faraday Society 67 (1971) 128.
[38] A.J. Bard, L.R. Faulkner, Electrochemical Methods Fundamentals and Applications, John Wiley & Sons, New York, 1980.
[39] A. Kudo, K. Omori, H. Kato, Journal of the American Chemical Society 121 (1999) 11459.
[40] A. Mills, A. Green, Journal of Photochemistry and Photobiology A 59 (1991) 191.
[41] N.Z. Bao, L.M. Shen, T. Takata, K. Domen, Chemistry of Materials 20 (2008) 110.